Multidimensional Dipolar Exchange-Assisted Recoupling Measurements in Solid-State NMR

3 AUTHORS, INCLUDING:

Joseph R. Sachleben
University of Chicago
33 PUBLICATIONS   **728** CITATIONS

SEE PROFILE

Lucio Frydman
Weizmann Institute of Science
220 PUBLICATIONS   **6,165** CITATIONS

SEE PROFILE

Multidimensional Dipolar Exchange-Assisted Recoupling Measurements in Solid-State NMR

Joseph R. Sachleben,[1] Peter Beverwyk,[2] and Lucio Frydman[3]

Department of Chemistry (M/C 111), University of Illinois at Chicago, 845 West Taylor Street, Chicago, Illinois 60607-7061

A series of uni- and multidimensional variants of the *di*polar *ex*change-*a*ssisted *r*ecoupling (DEAR) NMR experiment is described and applied to determinations of ^{13}C–^{14}N dipolar local field spectra in amino acids and dipeptides. The DEAR protocol recouples nearby nuclei by relying on differences in their relative rates of longitudinal relaxation, and has the potential to give quantitative geometric results without requiring radiofrequency pulsing on both members of a coupled spin pair. One- and two-dimensional variants of this recoupling strategy on generic *I–S* pairs are discussed, and measurements of ^{13}C–^{14}N distances and 2D local field experiments sensitive to the relative orientation of CN vectors with respect to the ^{13}C shielding tensor are presented. Since these measurements did not involve pulsing on the broad nitrogen resonance, their results were independent of the quadrupolar parameters of this nucleus. High-resolution 3D NMR versions of the 2D experiments were also implemented in order to separate their resulting local field patterns according to the isotropic shifts of inequivalent ^{13}C sites. These high-resolution 3D acquisitions involved collecting a series of 2D DEAR NMR data sets on rotating samples as a function of spinning angle, and then subjecting the resulting data to a processing akin to that involved in variable-angle correlation NMR. Once successfully tested on L-alanine this experiment was applied to the analysis of a series of dipeptides, allowing us to extract separate local field ^{13}C–^{14}N spectra from this type of multisite systems.   © 2000 Academic Press

Key Words: solid-state NMR; dipolar couplings; multidimensional spectroscopy; isotropic–anisotropic correlations.

INTRODUCTION

Solid-state nuclear magnetic resonance (NMR) has developed into a versatile tool for analyzing the structure of solids (*1*). This has been largely a consequence of progress in the development of new methods for increasing the sensitivity of the NMR experiment, of new techniques for producing highly resolved spectra from powders, and of new approaches for measuring meaningful parameters such as orientation or chemical environment. Dipolar couplings, which depend in a well-defined fashion on internuclear distances, have been particularly important for facilitating NMR determinations of structures in a wide variety of solid systems including synthetic polymers, biomolecules, and inorganic glasses (*2–4*). These developments started decades ago with the introduction of the *s*pin-*e*cho *do*uble-*r*esonance or SEDOR technique, which can discriminate single-spin (local) from two-spin dipolar interactions (*5, 6*), and during subsequent years they have been further stimulated by the development of a number of homo- and heteronuclear alternatives suitable for either static or spinning sample cases (*2, 7–14*). A common requirement among most heteronuclear dipolar characterizations is the need to irradiate with radiofrequency (RF) pulses both members of the coupled spin pair in an accurately and well-controlled fashion. This demand may be hard to satisfy when dealing with broad resonances such as those arising from quadrupolar nuclei, whose tensor parameters are not always *a priori* known or amenable to accurate manipulations.

Recently we have presented preliminary examples for an alternative to quantitative determinations of heteronuclear dipolar couplings dubbed *di*polar *ex*change-*a*ssisted *r*ecoupling (DEAR), which achieves a purely dipolar evolution by exploiting differences in relaxation rates among the coupled nuclei (*15*). This makes the approach particularly suitable for dealing with spin pairs possessing a fast-relaxing quadrupolar member attached to a more slowly relaxing spin-$\frac{1}{2}$, as dipolar couplings can then be extracted quantitatively without ever pulsing on the quadrupolar spin or having to know its field gradient characteristics. This contribution presents a more detailed report on the use of this technique, as well as new extensions to correlate the dipolar coupling measured with it to the relative orientations of the chemical shift tensor of the spin-$\frac{1}{2}$ partner. This in effect introduces a novel form of separate local field spectroscopy, which can measure along one of its dimensions the dipolar pattern between a spin-$\frac{1}{2}$ and a quadrupolar nucleus. The feasibility

of this experiment is demonstrated with a series of 2D NMR acquisitions on static and spinning L-alanine samples, which focused on the ^{13}C–^{14}N spin pair and could orient the C–N bond direction with respect to the principal axis of the ^{13}C chemical shift tensor. To enable the utilization of this experiment in samples of chemical or material interest, provisions for the inclusion of an additional high-resolution dimension capable of discriminating among chemically inequivalent nuclear environments were also developed. This three-dimensional rendering of the DEAR local field experiment achieved high resolution simply by scaling the chemical shift and dipolar anisotropies by means of variable-angle sample spinning; the resulting data were then processed following procedures similar to those previously described for variable-angle correlation spectroscopy (VACSY) (16). A number of examples of this 3D NMR experiment on natural-abundance molecules are demonstrated, and further potential refinements of these approaches are briefly discussed.

THEORY

General background. One of the requirements for the successful measurement of small heteronuclear dipolar couplings is the removal of other interactions such as the local chemical shift anisotropy (CSA) from the effective spin evolution determining the spectrum. The usual Hamiltonian encountered in this type of situation can thus be written as (17)

$$H = [\omega_{iso} + \delta(\Omega)]S_z + \omega_D(\Omega')2I_zS_z, \quad [1]$$

where ω_{iso} and $\delta(\Omega)$ are the isotropic and anisotropic chemical shift components of the spin being observed (e.g., a ^{13}C), and $\omega_D(\Omega')$ represents the *IS* dipolar coupling to be measured. The traditional strategy employed to obtain a purely dipolar spectrum derives from the SEDOR sequence shown in Fig. 1A; this involves an initial excitation followed by an evolution period $t_1/2$, synchronous *I* and *S* π-pulses that invert S_z but leave $2I_zS_z$ unchanged, and a final $t_1/2$ period of free evolution. At the end of this period the contributions of ω_{iso} and δ cancel while those of ω_D coherently add up, leading to a purely dipolar evolution of the *S* spin. A "universal" function describing this dipolar SEDOR evolution as a function of t_1 can be derived for arbitrary spin numbers and is given by

$$S(t_1)/S\,(t_1 = 0) = \langle S/S_0 \rangle(t_1)$$

$$= (2I + 1)^{-1} \sum_{m=-I}^{I} \cos[2\pi m\omega_D t_1], \quad [2]$$

where the ω_D's are to be weighted over all possible orientations.
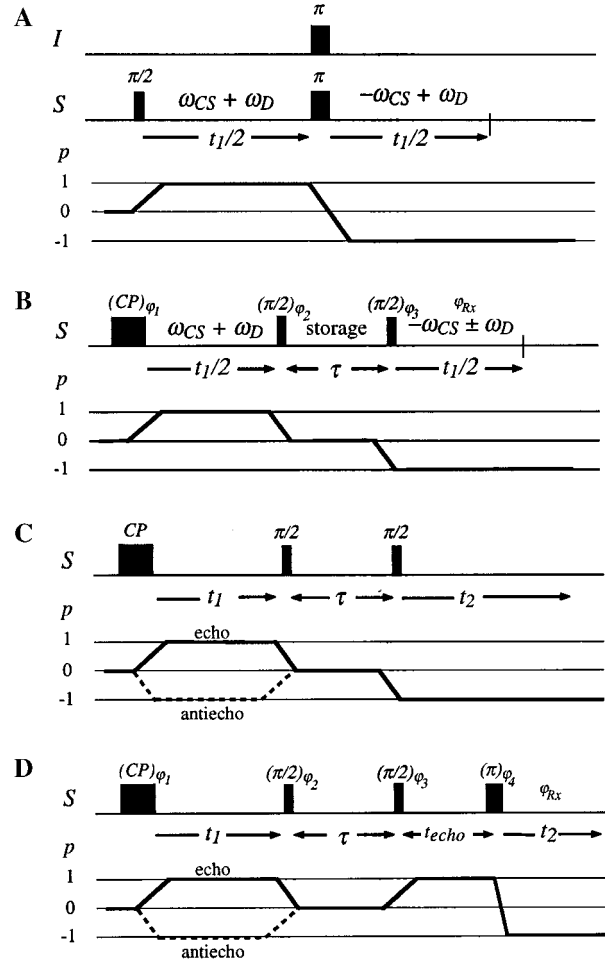

FIG. 1. Pluse strategies associated with double-resonance and exchange-assisted recoupling. Pulse lengths are indicated by rotation angles $\pi/2$ and π or by cross polarization (CP); pulse phases were cycled as summarized in Table 1 in order to select the relevant coherence pathway diagrams shown underneath each sequence. (A) Regular SEDOR experiment. (B) One-dimensional DEAR version, with the *I*-spin longitudinal relaxation during τ acting as a recoupling mechanism between the *I* and *S* spins. (C) 2D separated local field DEAR experiment for orienting the *I*–*S* vector with respect to the *S* principal axis shielding system. (D) 2D shifted-echo DEAR experiment for obtaining local field spectra without dead-time complications.

A similar evolution can be imparted on the *S* spin without applying *I*-spin irradiation if the two nuclear species possess different longitudinal relaxation times: $T_1^I < T_1^S$. Examples of pulse sequences that can then be employed to achieve a purely dipolar encoding are shown in Figs. 1B–1D; these sequences derive from 2D exchange NMR (18, 19) and form the basis of the experiments described in this work. As in SEDOR these sequences begin with an initial free evolution period; this is followed by a storage delay τ which, lasting an interval on the order of T_1^I, results in the microscopic randomization of I_z while producing only a minor attenua-

TABLE 1
Phase Cycles for Different DEAR NMR Experiments
Introduced in Fig. 1

Pulse	Phase

Phase cycle for 1D DEAR NMR (Fig. 1B)

φ_1	x	y	$-x$	$-y$	x	y	$-x$	$-y$	x	y	$-x$	$-y$	x	y	$-x$	$-y$
φ_2	x	x	x	x	y	y	y	y	$-x$	$-x$	$-x$	$-x$	$-y$	$-y$	$-y$	$-y$
φ_3	x	x	x	x	x	x	x	x	x	x	x	x	x	x	x	x
φ_{Rx}	x	$-y$	$-x$	y	y	x	$-y$	$-x$	$-x$	y	x	$-y$	$-y$	$-x$	y	x

Phase cycle for 2D shifted-echo DEAR NMR, echo pathway (Fig. 1D)

φ_1	x	y	$-x$	$-y$	x	y	$-x$	$-y$	x	y	$-x$	$-y$	x	y	$-x$	$-y$
φ_2	x	x	x	x	x	x	x	x	x	x	x	x	x	x	x	x
φ_3	x	x	x	x	y	y	y	y	$-x$	$-x$	$-x$	$-x$	$-y$	$-y$	$-y$	$-y$
φ_4	x	x	x	x	x	x	x	x	x	x	x	x	x	x	x	x
φ_{Rx}	x	y	$-x$	$-y$	$-y$	x	y	$-x$	$-x$	$-y$	x	y	y	$-x$	$-y$	x

Phase cycle for 2D shifted-echo DEAR NMR, antiecho pathway (Fig. 1D)

φ_1	x	y	$-x$	$-y$	x	y	$-x$	$-y$	x	y	$-x$	$-y$	x	y	$-x$	$-y$
φ_2	x	x	x	x	x	x	x	x	x	x	x	x	x	x	x	x
φ_3	x	x	x	x	y	y	y	y	$-x$	$-x$	$-x$	$-x$	$-y$	$-y$	$-y$	$-y$
φ_4	x	x	x	x	x	x	x	x	x	x	x	x	x	x	x	x
φ_{Rx}	x	$-y$	$-x$	y	$-y$	$-x$	y	x	$-x$	y	x	$-y$	y	x	$-y$	$-x$

tion of S_z, and is concluded by a reversal in the apparent sense of the S-spin precession. The stimulated echo that then forms refocuses the local but not the two-spin interactions, leading to a net dipolar evolution by exclusive irradiation of the S spins.

To formulate a concise description of the results afforded by DEAR experiments it is convenient to assume that the IS spin system is solely coupled by a dipolar interaction, that no homonuclear dipolar couplings among the I or S spins are present, and that T_1^I—even if shorter than T_1^S—is still long compared to the various transverse evolution times involved (e.g., t_1). It is then possible to describe the density matrix of the IS system as a sum of S-spin operators parameterized according to the z component m of the I-spin angular momentum, i.e.,

$$\rho(t) = (2I + 1)^{-1} \sum_{m=-I}^{I} \sum_{i=1}^{n} a_m^i S_i^{(m)}, \qquad [3]$$

where the summation over i corresponds to a sum over the complete set of operators describing the state of the S spin (for example, in a spin-$\frac{1}{2}$ system such complete sets could be $\{S_x, S_y, S_z\}$ or $\{S_+, S_-, S_o\}$). The dipolar exchange-assisted recoupling relies on monitoring the probability that a given z component of the S spin, $S_z^{(m)}$, shall become a different component $S_z^{(n)}$ due to the longitudinal relaxation of I. This relaxation process can be described classically by a $(2I + 1) \times (2I + 1)$ exchange matrix $\mathbf{K}$ via the relation (20)

$$\frac{d\mathbf{S}_z}{dt} = -\mathbf{K} \cdot \mathbf{S}_z \qquad [4]$$

which couples the various components in the vector $(S_z^{(-I)}, \ldots, S_z^{(I)})$. Equation [4] can be formally integrated over the storage interval τ as

$$\mathbf{S}_z(\tau) = e^{-\mathbf{K}\tau} \cdot \mathbf{S}_z(0) = \sum_{n=-I}^{I} \sum_{m=-I}^{I} e^{-K_{n,m}\tau} S_z^{(m)} \hat{n}, \qquad [5]$$

where $\{\hat{n}\}$ denote the basis operators. If it is assumed that single-quantum processes dominate the I-spin relaxation the exchange matrix takes the simplified form

$$K_{i,j} = \begin{cases} 1/T_1^I & \text{if } i = j \pm 1 \\ \dfrac{1}{T_1^S} - \displaystyle\sum_{l \neq m} K_{l,m} & \text{if } i = j \\ 0 & \text{otherwise.} \end{cases} \qquad [6]$$

In this limit $\mathbf{K}$ is a tridiagonal matrix very similar to those encountered in Hückel's molecular orbital treatment of conjugated olefins (21). Borrowing from results known in this area it becomes possible to exactly diagonalize the exchange matrix $\mathbf{K}$ for arbitrary spin numbers I; its eigenvalues are given by

$$\lambda_k = \frac{1}{T_1^S} + \frac{2}{T_1^I} \left[1 + \cos\left(\frac{k\pi}{2I+1}\right) \right],$$
$$k = 1, \ldots, 2I + 1 \quad [7]$$

and the corresponding eigenvectors are

$$u_{-I}^{(k)} = \sqrt{1 - \sum_{m=-I+1}^{I} u_m^{(k)} u_m^{(k)}} \qquad [8a]$$

$$u_{-I+1}^{(k)} = -\left[1 + 2 \cos\left(\frac{k\pi}{2I+1}\right) \right] u_{-I}^{(k)} \qquad [8b]$$

$$u_{-I+j}^{(k)} = -\left[u_{-I+j-2}^{(k)} + 2 \cos\left(\frac{k\pi}{2I+1}\right) u_{-I+j-1}^{(k)} \right],$$
$$2 \leq j \leq 2I. \quad [8c]$$

With these expressions it is possible to derive the operator $\mathbf{P} = e^{-\mathbf{K}t}$ describing the probability that the m quantum number of I has changed from i to j value during the storage period τ of an exchange experiment; its elements are

$$P_{i,j}(\tau) = \sum_{k=1}^{2I+1} e^{-\lambda_k \tau} u_i^{(k)} u_j^{(k)}, \quad I \leq i, j \leq 2I + 1. \quad [9]$$

This relaxation-driven probability matrix simplifies considerably in the limit of complete exchange, when the storage time τ is long with respect to T_1^I but short compared to T_1^S. This limit is to be expected when S is a dilute spin-$\frac{1}{2}$ nucleus such as ^{13}C or ^{15}N, and I is fast relaxing due to strong quadrupolar coupling (a ^{14}N or a ^{59}Co). The eigenvalues $\{\lambda_k\}_{1 \leq k \leq 2I+1}$ then have the property that $\lambda_{2I+1} = 1/T_1^S$ while all other eigenvalues depend on T_1^I. This implies that for $T_1^I \ll \tau$

$$e^{-\lambda_k \tau} \begin{cases} \rightarrow 0, & k = 1, \ldots, 2I \\ e^{-\tau/T_1^S}, & \text{for } k = 2I + 1. \end{cases} \quad [10]$$

The eigenvector corresponding to the $k = 2I + 1$ eigenvalue possesses in this limit all coefficients equal to $1/\sqrt{2I+1}$. Therefore the probability matrix elements are simply

$$P_{i,j}(\tau) = \frac{1}{2I+1} e^{-\tau/T_1^S}, \quad 1 \leq i, j \leq 2I + 1, \quad [11]$$

reflecting the fact that when the storage time is long compared to the relaxation time of the I spins the exchange probability gets equalized among the $2I + 1$ states defining S in the two-spin space.

With this background in hand it becomes straightforward to calculate the signals obtained for a number of different variants of the DEAR NMR experiments; these calculations are presented below for arbitrary spin numbers of the I–S pairs.

Unidimensional NMR experiments. Figure 1B illustrates a simple approach for measuring dipolar I–S couplings by monitoring in a pointwise manner the intensities observed in a 1D stimulated-echo experiment. To calculate the resulting NMR signal we follow the conventions of the previous paragraph; the spin density matrix evolved during its first $t_1/2$ period can then be written as

$$\rho\left(\frac{t_1}{2}\right) = (2I + 1)^{-1} e^{-i(\omega_{iso}+\delta)t_1/2} \sum_{m=-I}^{I} e^{-im\omega_D t_1/2} S_+^{(m)}. \quad [12]$$

After the storage period τ, when the S magnetization was placed along the external magnetic field and I spins were allowed to relax and randomize the z component of their spin angular momentum, we obtain

$$\rho(\tfrac{1}{2} t_1, \tau) = (2I + 1)^{-1} e^{-i(\omega_{iso}+\delta)t_1/2}$$

$$\times \sum_{m=-I}^{I} \sum_{n=-I}^{I} e^{-im\omega_D t_1/2} P_{m,n}(\tau) S_z^{(n)}. \quad [13]$$

Finally, after a second $t_1/2$ period with the effective S evolution reversed, the chemical shift echoes and we have

$$\rho(t_1, \tau) = (2I + 1)^{-1} \sum_{m=-I}^{I} \sum_{n=-I}^{I} e^{-i(m-n)\omega_D t_1/2} P_{m,n}(\tau) S_-^{(n)}. \quad [14]$$

The normalized magnetization measurable at this time is therefore

$$\langle S/S_0 \rangle(t_1) = \text{Tr}\{\rho(t_1, \tau) S_+\}$$

$$= (2I + 1)^{-1} \left[\sum_{k=-I}^{I} P_{k,k}(\tau) \right.$$

$$\left. + \sum_{k=-I}^{I} \sum_{\Delta k>0}^{I+k} 2 P_{k,k+\Delta k}(\tau) \cos(\tfrac{1}{2}\Delta k \omega_D t_1) \right], \quad [15]$$

where $\Delta k = m - n$ and the identities $[P_{k,k-\Delta k} = P_{k,k+\Delta k} = P_{k-\Delta k,k} = P_{k+\Delta k,k}]$ were used. The first summation in this expression for $\langle S/S_0 \rangle$ describes those spins whose neighbors did not change quantum state during the storage; the contribution of these spins refocuses completely and is consequently uninteresting. By contrast the double summation represents spins whose neighbors made a Δk quantum change during the storage period; these S spins contribute to a purely dipolar dephasing.

It is illustrative to consider the simple yet fairly common complete randomization limit, as then "universal" dipolar dephasing curves independent of the I-spin relaxation and solely a function of $\omega_D \cdot t_1$ will result. In this limit Eq. [15] becomes

$$\langle S/S_0 \rangle(t_1) = (2I + 1)^{-1} \left[1 + \frac{2}{2I + 1} \right.$$

$$\left. \times \sum_{\Delta k=1}^{2I} (2I + 1 - \Delta k) \cos\left(\frac{1}{2}\Delta k \omega_D t_1\right) \right]. \quad [16]$$

Figure 2 illustrates some of these curves for different I-spin numbers; as expected they all show a decay and oscillation
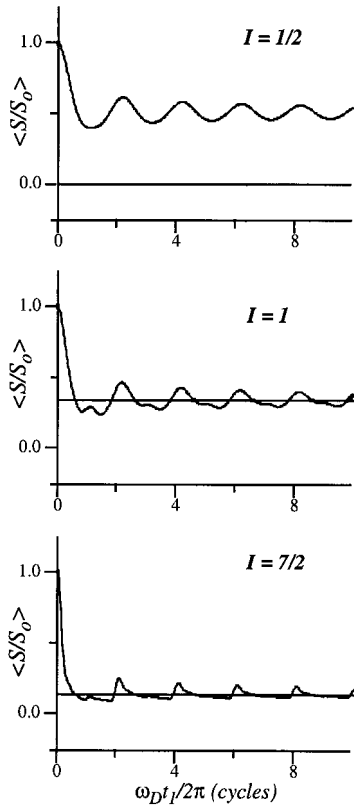
FIG. 2. Comparison between the normalized dipolar dephasing curves expected from fully randomized exchange experiments versus the ideal SEDOR limiting values (—), as a function of the dephasing phase $\omega_D \cdot t_1$ for different spin numbers I.

around the $(2I + 1)^{-1}$ value arising from the $P_{k,k}$ sum. This value compares unfavorably with the decay observed when using SEDOR for the case $I = \frac{1}{2}$ as then $\langle S/S_0 \rangle$ can dephase all the way to zero, yet it becomes competitive when considering $I \geq 1$. Furthermore, since in these quadrupolar cases the ideal SEDOR expectation may be hard to achieve or quantify by virtue of the large I spectral linewidths, the application of exchange-assisted recoupling strategies appears particularly convenient for this type of cases.

Bidimensional separate local field experiments. The unidimensional pointwise scheme of the previous paragraph can be extended to obtain not only dipolar $I–S$ information, but also a correlation between this coupling tensor and nondipolar fields affecting the S-spin evolution such as the chemical shift anisotropy. A 2D NMR sequence like that in Fig. 1C can retrieve such correlation, as in it identical shielding but different dipolar frequencies operate during the evolution and the acquisition times. To calculate the actual 2D NMR signals afforded by this sequence we follow similar guidelines as above; the spin propagation over t_1, the mixing period τ, and t_2 yields

$$\rho(t_1, \tau, t_2) = (2I + 1)^{-1} e^{-i(\omega_{iso} + \delta)(t_1 - t_2)}$$

$$\times \sum_{m=-I}^{I} \sum_{n=-I}^{I} e^{-i\omega_D(mt_1 - nt_2)} P_{m,n}(\tau) S_-^{(n)}.$$

[17]

The expectation value of the S magnetization is then

$$\langle S/S_0 \rangle(t_1, \tau, t_2) = (2I + 1)^{-1} e^{-i(\omega_{iso} + \delta)(t_1 - t_2)}$$

$$\times \sum_{m=-I}^{I} \sum_{n=-I}^{I} P_{m,n}(\tau) e^{-i\frac{1}{2}(m+n)\omega_D(t_1 - t_2)}$$

$$\times e^{-i\frac{1}{2}(m-n)\omega_D(t_1 + t_2)},$$

[18]

showing the explicit dipolar/(shielding + dipolar) correlation obtained on viewing this signal as a function of the sheared $(t_1 + t_2)/(t_1 - t_2)$ variables, respectively. This equation also highlights that besides the major echo at $t_2 = t_1$ subsidiary dipolar echoes will form when $t_2 = \frac{m}{n} t_1$, where m and n are the quantum states of the fast relaxing spin during t_1 and t_2 (and m, $n \neq 0$). Also worth noting is the fact that Eq. [18] can be cast into an amplitude-modulated dipolar form similar to Eq. [16] by replacing $k = n$, $\Delta k = m - n$:

$$\langle S/S_0 \rangle(t_1, \tau, t_2) = (2I + 1)^{-1} e^{-i(\omega_{iso} + \delta)(t_1 - t_2)}$$

$$\times \left\{ \sum_{k=-I}^{I} P_{k,k}(\tau) \cos[k\omega_D(t_1 - t_2)] \right.$$

$$+ \sum_{k=-I}^{I} \sum_{\substack{\Delta k=-I-k \\ \Delta k \neq 0}}^{I-k} 4 P_{k,k+\Delta k} \cos[\frac{1}{2}\Delta k \omega_D(t_1$$

$$\left. + t_2)] \cos[(k + \frac{1}{2}\Delta k)\omega_D(t_1 - t_2)] \right\}.$$

[19]

Because of potential mixed-phase distortions and dead-time problems that can arise on using the sequence in Fig. 1C, we found it convenient to consider also a shifted-echo version of this local field DEAR experiment. The pulse sequence for this 2D shifted-echo DEAR is shown in Fig. 1D. Propagation of the density matrix over the t_1, storage, echo, and t_2 time intervals under the assumption $t_{echo} \ll T_1^I$ now gives

$$\rho(t_1, \tau, t_{echo}, t_2) = e^{-i(\omega_{iso} + \delta)(t_{echo} - t_2)} \sum_{m=-I}^{I} \sum_{n=-I}^{I}$$

$$\times e^{\frac{1}{2}(m-n)\omega_D t_1} e^{i\frac{1}{2}n\omega_D(t_{echo} - t_2)} P_{m,n}(\tau) S_-^{(n)}.$$

[20]

Using a derivation analogous to the one leading from Eq. [17] to Eq. [19], the expectation value of the magnetization resulting for this experiment can be written as

$$\langle S/S_0 \rangle (t_1, \tau, t_2)$$

$$= (2I + 1)^{-1} e^{-i(\omega_{iso} + \delta)(t_{echo} - t_2)}$$

$$\times \left\{ \sum_{k=-I}^{I} P_{k,k}(\tau) \cos[k\omega_D(t_{echo} - t_2)] \right.$$

$$+ \sum_{k=-I}^{I} \sum_{\substack{\Delta k = -I-k \\ \Delta k \neq 0}}^{I-k} P_{k,k+\Delta k}(\tau) \left\{ \cos[k\omega_D(t_{echo} \right.$$

$$- t_2)] \cos\left[\frac{1}{2} \Delta k \omega_D t_1 \right] + \sin[k\omega_D(t_{echo} - t_2)]$$

$$\left. \left. \times \sin\left[\frac{1}{2} \Delta k \omega_D t_1 \right] \right\} \right\}. \qquad [21]$$

This expression is similar to Eq. [19] except for the appearance of additional sine terms, arising because no effective π pulse is applied to the fast relaxing I spins at the end of the echo time.

High-resolution 3D local field experiments. The 2D NMR sequences described in the previous paragraph have the potential of extending to quadrupole-containing systems and in a simple fashion, acquisitions that have hitherto been confined mostly to heteronuclear spin-$\frac{1}{2}$ pairs. If several inequivalent S sites are present in the sample, however, one can expect the broad 2D local field patterns arising from these experiments to overlap and thereby prevent the extraction of useful information. For dealing with such multisite systems one would ideally like an NMR experiment capable of resolving the static-like dipolar/shielding 2D powder patterns along a third high-resolution spectral dimension, characterized solely by the isotropic shifts of S nuclei. During the past several years a number of alternatives have been proposed for carrying out such isotropic–anisotropic separations of interactions; these have included the use of rotor-synchronized multipulse experiments on spinning samples (*22*), interrupted spin evolutions on slowly rotating or hopping samples (*23–25*), or variable-angle spinning signal acquisitions. Because of its ease of implementation, high digital resolution along the isotropic dimension, and good signal-to-noise, the latter variable-angle correlation spectroscopy (VACSY) approach has already been successfully used in a number of 2D and 3D NMR acquisitions (*16, 26–30*). We decided to incorporate it into the specific case of the dipolar experiments hereby discussed in order to facilitate the resolution of the bidimensional DEAR local field lineshapes.

From the standpoint of a theoretical analysis the use of fast sample rotation requires modifying Eq. [1] into

$$\mathcal{H} = [\omega_{iso} + \delta(\Omega) P_2(\cos \theta)] S_z + \omega_D(\Omega') P_2(\cos \theta) 2I_z S_z,$$

$$[22]$$

where $P_2(\cos \theta) = (3 \cos^2\theta - 1)/2$ is a function of the angle θ between the axis of sample rotation and the external magnetic field, and the angular sets (Ω, Ω') define now the shielding and dipolar tensor orientations with respect to rotor (rather than the Zeeman) axes. All that the introduction of this sample spinning procedure requires is therefore scaling the anisotropic frequency terms in the equations of the preceding paragraphs by a factor $P_2(\cos \theta)$. To consider but the most involved of these cases, the signal arising from a VACSY/shifted-echo DEAR experiment (Eq. [21]) simply becomes

$$\langle S/S_0 \rangle (t_1, \tau_1, t_2, \theta) \qquad [23]$$

$$= (2I + 1)^{-1} e^{-i[\omega_{iso} + \delta P_2(\cos \theta)](t_{echo} - t_2)}$$

$$\times \left\{ \sum_{k=-I}^{I} P_{k,k} \cos[k\omega_D P_2(\cos \theta)(t_{echo} - t_2)] \right.$$

$$+ \sum_{k=-I}^{I} \sum_{\substack{\Delta k = -I-k \\ \Delta k \neq 0}}^{I-k} P_{k,k+\Delta k} \left\{ \cos[k\omega_D P_2(\cos \theta) \right.$$

$$\times (t_{echo} - t_2)] \cos\left[\frac{1}{2} \Delta k \omega_D P_2(\cos \theta) t_1 \right]$$

$$+ \sin[k\omega_D P_2(\cos \theta)(t_{echo} - t_2)]$$

$$\left. \left. \times \sin\left[\frac{1}{2} \Delta k \omega_D P_2(\cos \theta) t_1 \right] \right\} \right\}. \qquad [23]$$

By distinguishing the isotropic from the anisotropic components of the interactions, the spinning angle θ introduces the additional degree of freedom required for the 3D NMR separation. Rather than viewing this signal as a function of the experimental acquisition variables (t_1, t_2, θ), however, the VACSY protocol views it in terms of the "extraction" variables which encode the isotropic frequency ω_{iso}, the DEAR dipolar powder pattern, and the sum of this powder pattern plus the shielding anisotropy, respectively. For the case of Eq. [23] these would be

$$t_a = t_{echo} - t_2, \quad t_b = P_2(\cos \theta) t_1, \quad t_c = P_2(\cos \theta)(t_{echo} - t_2),$$

$$[24]$$

and it is against these variables that the variable-angle data are Fourier transformed. This implies that just as in the static case, DEAR dipolar/shielding powder patterns with effective dipolar coupling constants $\frac{1}{2} \Delta k \omega_D$, $1 \leq \Delta k \leq 2I + 1$, will be extracted. No further description of the anisotropic lineshapes
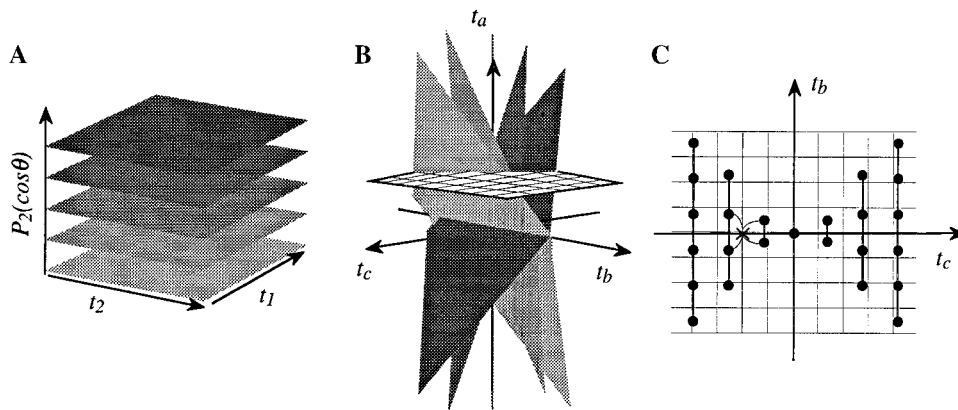
FIG. 3. Stages involved in the acquisition of VACSY-based high-resolution 3D separate local field spectra. (A) 2D time-domain exchange data are initially collected as a function of the axis of sample spinning using, for instance, the shifted-echo alternative shown in Fig. 1D. (B) These data are then rearranged into their correct position in the (t_a, t_b, t_c) space defined in Eq. [24]. (C) Points are evenly spaced along the isotropic t_a axis but obtaining a regular grid of data ready to be fast Fourier transformed requires interpolating the sampled points within each (t_b, t_c) plane.

is consequently needed: the implementation of this 3D VACSY/DEAR procedure simply resolves static-like patterns according to each site's isotropic shift.

DATA PROCESSING AND EXPERIMENTAL

Computing and data processing. The acquisition alternatives described in the preceding section were experimentally assayed. The uni- and bidimensional data sets were processed on PowerPC computers using either MacNMR or the RMN software programs (*31, 32*). The three-dimensional data were processed on Unix workstations (Silicon Graphics R3000 or Sun UltraSparc) using C++ code specially written for carrying out a multidimensional NMR data interpolation onto a regular grid of points and its subsequent Fourier processing. Final visualization of these spectra was performed either on the Silicon Graphics computer using IRIS Explorer modules or on the Sun computer using custom-written programs based on the POV graphic library. The processing of the 3D data sets was carried out in several steps (Fig. 3). First, a series of 2D exchange NMR signals $\langle S \rangle(t_1, t_2)$ was collected for fixed values of $P_2(\cos \theta)$. These data were then stored along with their unique sets of experimental coordinates (t_1, t_2, θ), and employed to interpolate a regular 3D grid of points equally distributed in the "natural" Fourier space defined by Eq. [24]. Given the linear dependence that in this case the parameter t_a has on the acquisition time t_2, all data could be distributed along equally spaced planes of points provided that the condition $\Delta t_a = \Delta t_2$ was chosen upon setting an experiment. The patterns that the digitized data points then subtended in these planes are shown in Fig. 3; also shown are the principles involved in the subsequent interpolation of the sampled data onto the final regular grid of points. Basically, this procedure required finding for each coordinate in the (t_a, t_b, t_c) grid its

four nearest sampled data, and then use the latter to compute the expected grid value based on simple distance considerations. Since the sampling of these planes was in general incomplete only points within the experimentally scanned regions were interpolated. A further precaution that was taken prior to beginning this interpolation was to average the values of multiple experimental points possessing identical (t_a, t_b, t_c) coordinates, arising as a consequence of having used constant ΔP_2, Δt_1, and Δt_2 increments. To give a better idea of the overall characteristics of this procedure, a typical 3D VACSY/DEAR NMR experiment involved acquiring $\approx 161,000$ data points, which were in turn used to interpolate about $\frac{1}{3}$ of the volume occupied by a $512 \times 48 \times 48$ (t_a, t_b, t_c) points array. The suitability of this interpolation procedure was tested extensively on simulations based on typical ^{13}C–^{14}N coupling and shielding parameters prior to the implementation of the actual experiments. The C++ source code for carrying out this type of 3D data interpolation for arbitrary functionals of (t_a, t_b, t_c) depending on any number of experimental variables is available upon request.

NMR experiments. NMR acquisitions were carried out on natural-abundance samples of L-alanine, L-glycyl-L-alanine, L-alanyl-L-alanine, and L-alanyl-L-aspartic acid, purchased from Aldrich and used without further purification. For both the static and spinning experiments these samples were packed into standard 5-mm Zirconia MAS spinners (Doty Sci.) and placed into a doubly tuned laboratory-built dynamic-angle-spinning NMR probehead. Experiments were then run monitoring the ^{13}C signal at 7.1 T (75.8 MHz Larmor frequency) on a laboratory-built spectrometer controlled by a Tecmag Inc. pulse programmer and equipped with high-power RF components. The ^1H decoupling field strengths employed in the experiments were typically greater than 75 kHz, while ^{13}C $\pi/2$
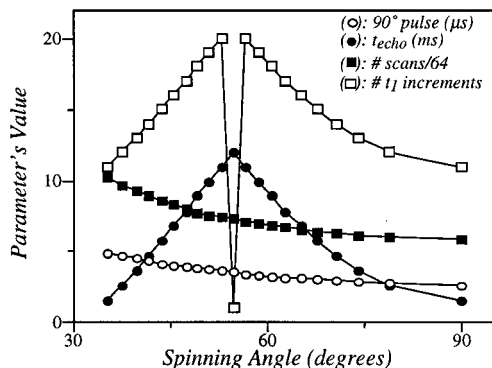
FIG. 4. Depiction of how different experimental parameters involved in the 3D VACSY NMR acquisitions were varied to account for the changing spinning angle θ, which was also the angle between the RF coil and the external magnetic field. In addition to these changes, the number of points collected during t_2 was doubled (to 512) for the five experiments neighboring the magic axis.

storage pulses were 2.7 μs long. The spinning sample experiments also incorporated a ramped cross-polarization sequence with contact times of 1–2 ms to ensure the homogeneous excitation of nuclei in all crystallites even at the moderately fast rates employed (8–10 kHz, fast enough to neglect spinning-related complications) (33). For the 2D shifted-echo experiments typical acquisitions involved exchange times $\tau \approx$ 0.5–2 s, 1-ms t_{echo} delays (much larger than the 80-μs dead times), recycle delays of 1–2 s, 128 scans, and 4-kHz/30-kHz spectral widths along the dipolar and chemical shift dimensions, respectively. In an effort to further eliminate mixed-phase artifacts, data from both echo and antiecho pathways were collected in the 2D experiments (16 t_1 points for each) (34); these sets were then combined and zero-filled to 128 points prior to Fourier processing. For the three-dimensional acquisitions many of these 2D shifted-echo timing and acquisition parameters were kept constant; the main difference of course was that a series of 2D data sets had now to be collected as a function of spinning angle. These consisted of 21 different orientations of the rotor axis corresponding to evenly spaced steps in $P_2(\cos \theta)$ between -0.5 and $+0.5$ (35.3° ≤ θ ≤ 90°), set in turn by an intelligent stepping motor controller system governed by the spectrometer's pulse programmer. Since the sample RF coil in the probehead was kept coaxial with the sample spinning direction, the efficiency of both the irradiation and the detection changed with the spinning axis chosen. This was compensated by varying as $\sin^{-1}\theta$ both the number of scans and the pulse widths for each of the spinning angles. Inspection of the relevant 3D time domain sampled during the course of the experiments (Fig. 3B) also suggested additional potential refinements worth incorporating. For instance, the fact that dipolar patterns were encoded by the $P_2(\cos \theta) \cdot t_1$ function implied that acquisition of echo and antiecho data at both positive and negative $P_2(\cos \theta)$ values was redundant;

only one of these sets (the antiecho data) was consequently collected. Also, as the absolute value of $P_2(\cos \theta)$ decreases the signals' lifetime along both t_1 and t_2 is expected to lengthen; we consequently found it convenient to extend these evolution times (t_1, t_2) as well as the position of the shifted-echo maximum (t_{echo}) accordingly. Figure 4 summarizes these details by depicting how various experimental parameters were changed throughout the 2D variable-angle spinning acquisitions; notice the peculiar status of the MAS experiment arising due to the fact that at this angle no anisotropies are worth encoding. Other ^{13}C spectral parameters included an 11-kHz sampling width along the isotropic dimension, a 5-kHz width along the dipolar dimension, and a 30-kHz-wide shift anisotropy domain. The overall durations for these 3D NMR acquisitions ranged between 3 and 7 days. Once acquired, data were interpolated into a dense grid as described earlier with 512 points along the isotropic dimension and 48 × 48 points for the anisotropic ones. These arrays were suitably weighted, zero-filled to 512 × 128 × 128 points, and Fourier transformed to obtain the final spectra.

RESULTS AND DISCUSSION

To test the potential uses of the various DEAR versions discussed above a series of experiments focusing on the bonded ^{13}C–^{14}N spin pair of natural-abundance L-alanine was performed. This compound was chosen because of its good signal-to-noise and because of the possibility of easily resolving its three inequivalent carbon environments even when spinning at angles other than 54.7°. Figure 5A shows the
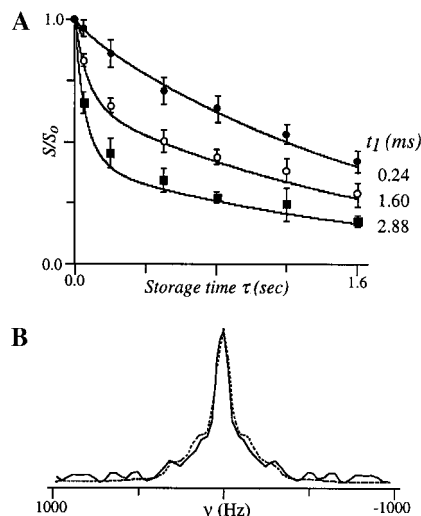

FIG. 5. Unidimensional DEAR NMR experiments on L-alanine done while spinning the sample at 66.7° with respect to the magnetic field. (A) C_α echo intensity as a function of storage and dephasing times; lines are the best fit of Eq. [15] to all data. (B) Fourier transform of echo tops collected in the complete randomization limit ($\tau = 1$ s) to get a purely dipolar C–N spectrum; the dotted line is an ideal simulation based on three suitably weighted ^{13}C Pake doublets.
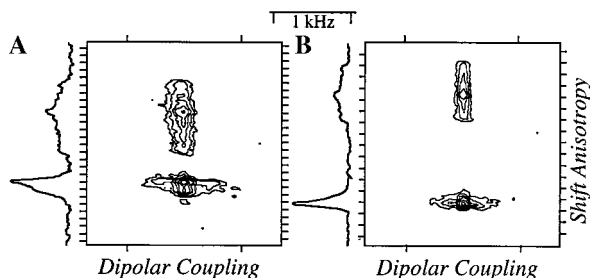
FIG. 6. Experimental 2D local field results obtained when applying the shifted-echo sequence (Fig. 1D, $\tau = 1$ s) to L-alanine: (A) static powder; (B) sample spinning at 90°. Vertical traces indicate the projections onto the chemical shift axes.

intensity observed for the C_α carbon resonance as a function of storage time τ and evolution time t_1, upon applying the 1D echo version shown in Fig. 1B while spinning the sample at 66.7° (at this angle all three sites are still resolved but the dipolar coupling has been reintroduced). To avoid potential artifacts the echo times of these experiments were chosen as multiples of the spinning sample rotor period, even if at the spinning rates employed this may not have been relevant. At short echo times the echo intensity decays with τ monoexponentially as a result of the $^{13}C_\alpha$ longitudinal relaxation. As the echo time increases, however, dipolar couplings are no longer averaged and the decay of the echo intensity becomes multiexponential. Figure 5 also shows the best simultaneous fit of

these echo intensities as a function of t_1 and τ by Eq. [15]. The scaling of the dipolar coupling by the spinner angle was explicitly included in the fit and the best-fit values were found to be $T_1^{13C}\alpha = 1.8 \pm 0.6$ s, $T_1^{14N} = 0.09 \pm 0.06$ s, and $r_{CN} = 1.5 \pm 0.3$ Å. The C–N distance compares favorably to the literature value of 1.487 Å (*35*), while the faster relaxation of the quadrupolar nucleus vis à vis the ^{13}C confirms the applicability premise mentioned above. In fact in the limit where τ is long compared to T_1^{14N} a Fourier transformation of the echo tops as a function of t_1 leads to a purely dipolar C–N spectrum (Fig. 5B). This consists of three Pake-type components (which in general will be $2I + 1$, Eq. [15]): one at zero frequency which arises from the $P_{k,k}$ terms, one with dipolar coupling $\frac{1}{2}\nu_D$ due to those ^{14}N's whose quantum number changed by ± 1, and another with dipolar coupling of ν_D due to those ^{14}N's whose Δm was ± 2.

These 1D dipolar measurements can be extended to two dimensions as shown in Figs. 1C and 1D; experimental 2D dipolar/chemical shift separated local field DEAR spectra arising by use of the latter sequence are shown in Fig. 6, again for the case of L-alanine in the complete randomization limit. The spectra clearly show the bigger CO anisotropy along the chemical shielding domain, the stronger C–N dipolar coupling for the α site, and the absence of a methyl peak due to its short longitudinal relaxation (comparable to that of the ^{14}N). Also characteristic is the reversal and scaling of all the anisotropies upon repeating the static experiment while rapidly spinning at an angle $\theta = 90°$, where $P_2(\cos\theta)$ goes from a value of 1 to -0.5. The fact that these spectra were acquired for $\tau \gg T_1^{14N}$ implies that their lineshapes can be analyzed without regard to the ^{14}N relaxation or quadrupolar properties, thus yielding sensitive information about the relative direction of the inter-
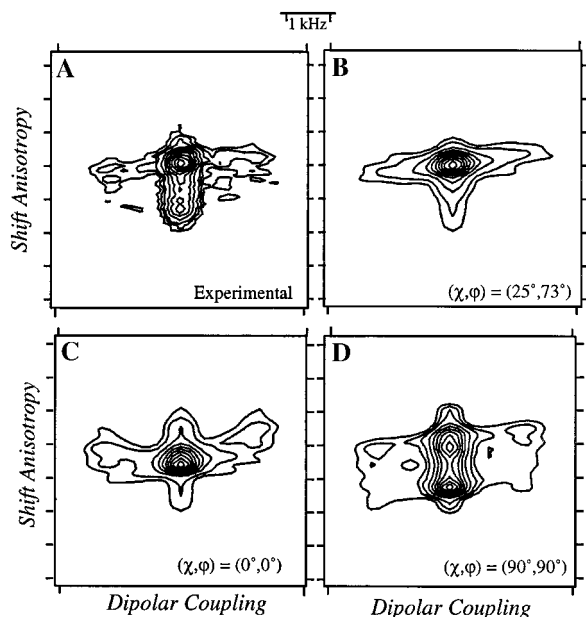

FIG. 7. Comparison between the experimental 2D shifted-echo DEAR pattern observed for the C_α site of static L-alanine and simulations calculated for different orientations (χ, φ) of the C–N vector; coupling parameters are $\Delta = -35$ ppm, $\eta = 0.2$, and $\omega_D = 2\pi \cdot 666$ rad/S.
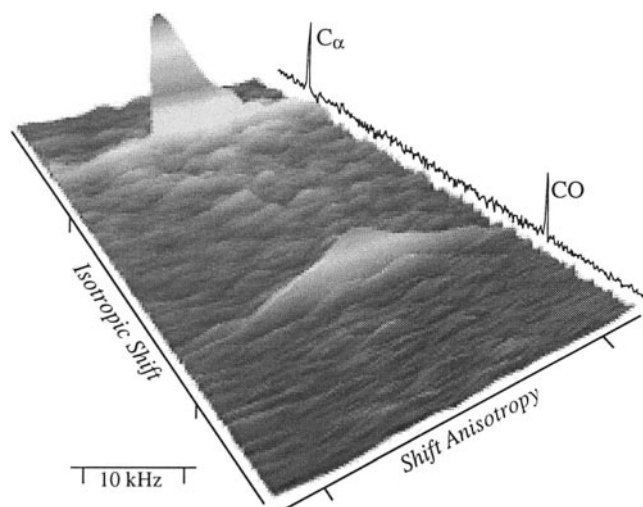

FIG. 8. Projection of the 3D VACSY/DEAR results obtained for L-alanine ($\tau = 1$ s) along the dipolar-encoding dimension; the result is a relaxation-weighted ^{13}C isotropic/anisotropic correlation spectrum.
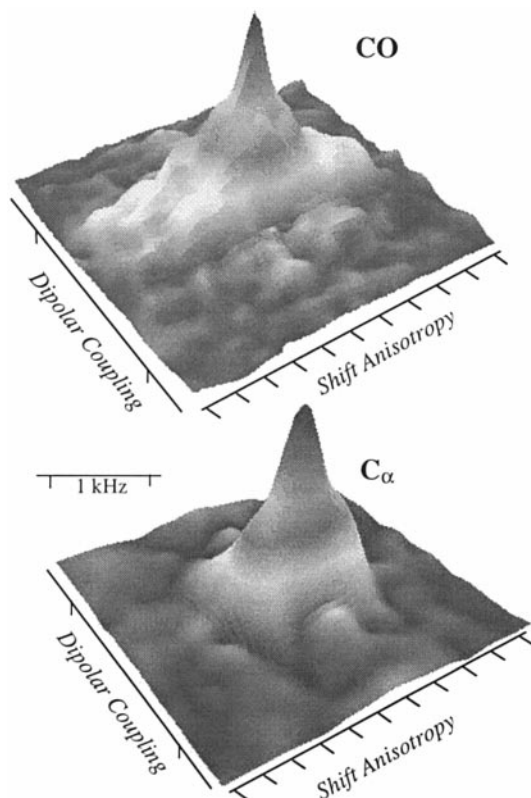
CO

C$_\alpha$

Dipolar Coupling

Shift Anisotropy

1 kHz

FIG. 9. Experimental ^{13}C NMR lineshapes extracted from a 3D VACSY/DEAR spectrum at the isotropic frequencies of L-alanine's C$_\alpha$ and CO sites. These dipolar/shielding local field powder patterns are equivalent to those presented in Fig. 6A.

$H_3\overset{+}{N}CH(CH_3)CONHCH(CH_3)CO_2^-$

CO$_2^-$

Coupling

CONH

Coupling

NHCH

Coupling

$H_3\overset{+}{N}CH$

Coupling

Shift Anisotropy

3 kHz

Isotropic Shift (ppm)

0   100   200

FIG. 10. Schematic representation of the 3D VACSY/DEAR NMR results obtained on an L-alanyl-L-alanine powder: the 1D slice is the projection of the 3D set onto the isotropic 13C axis; 2D powder lineshapes show the dipolar local field patterns extracted at the indicated isotropic frequencies. Storage and recycle delays of 1 s were employed in this acquisition.

nuclear vector with respect to the chemical shift principal axis system. Figure 7 compares this 2D experimental result on the C$_\alpha$ of a static L-alanine sample with a series of simulations calculated as a function of polar and azimuthal angles. These predictions illustrate the good match between the experimental powder lineshape and the results expected from the C–N orientation $(\chi, \varphi) = (25°, 73°)$ measured by McDowell and co-workers on an L-alanine single crystal (*36*).

Although alanine's sites are well resolved in static DEAR NMR experiments due to their different chemical nature, it is still convenient to use this compound as a test case for the implementation of the high-resolution 3D local field experiment. Examples of various projections and slices afforded by such 3D NMR acquisition are shown in Figs. 8 and 9. Projecting the 3D data along the dipolar dimension yields essentially a 2D NMR spectrum where alanine's static anisotropic powder patterns are separated along each sites' isotopic chemical shifts (even if the CH$_3$ group is absent due to its relaxation during the mixing), while slices extracted at the isotropic frequencies of the sites are essentially indistinguishable from the 2D local field spectra observed in the static exchange experiments. This agreement justifies the various considerations described above
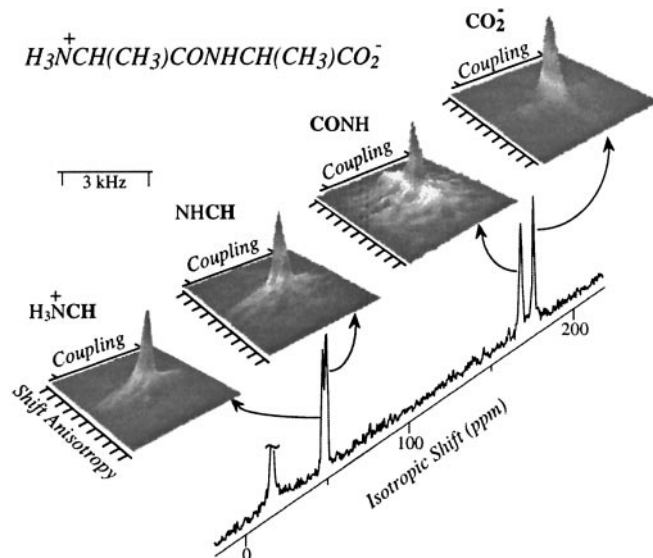
regarding our 3D data acquisition and processing protocol; the only minor artifacts characterizing the powder resonances in these 3D acquisitions are small diagonal ridges that arise from an incomplete sampling of all four quadrants of the (t_b, t_c) planes.

With this positive test of the high-resolution experiment in hand, a series of 3D VACSY/DEAR NMR acquisitions was carried out on several natural-abundance dipeptides; some of
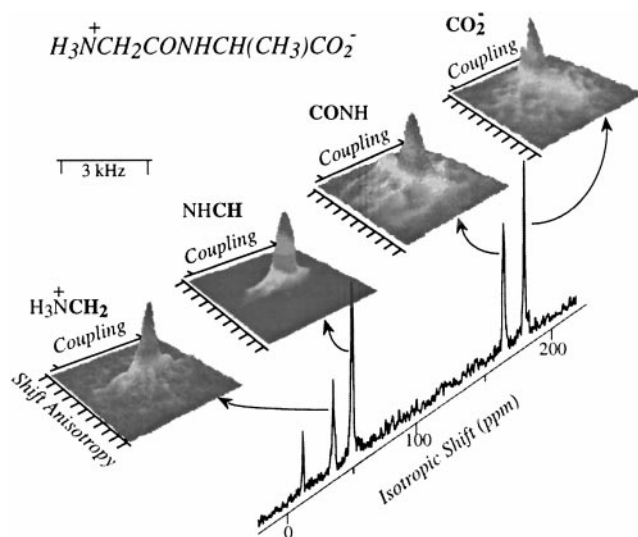

$H_3\overset{+}{N}CH_2CONHCH(CH_3)CO_2^-$

CO$_2^-$

Coupling

CONH

Coupling

NHCH

Coupling

$H_3\overset{+}{N}CH_2$

Coupling

Shift Anisotropy

3 kHz

Isotropic Shift (ppm)

0   100   200

FIG. 11. The same as in Fig. 10 but for L-glycyl-L-alanine, using 1.5 s storage and 1-s recycle delays.

$$H_3\overset{+}{N}CH(CH_3)CONHCH(CH_2CO_2H)CO_2^-$$
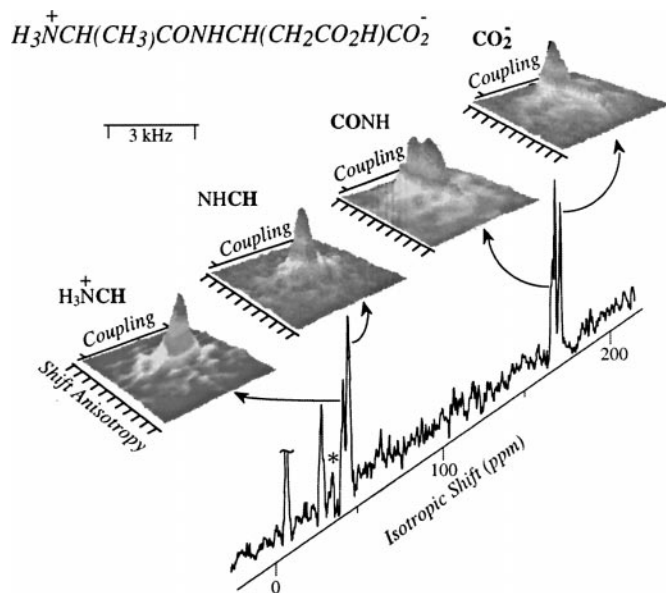
FIG. 12. The same as in Fig. 10 but for L-alanyl-L-aspartic acid using 2 s storage and 1-s recycle delays.

TABLE 2

Chemical Shift Anisotropy Parameters and CN Vector Orientations Extracted by Simulating the 3D Variable-Angle DEAR Slices Shown in Fig. 13 for L-Alanyl-L-alanine

Site	Δ (± 2 ppm)	η (± 0.1)	(χ, φ) ($\pm 15°$)
C_α (N-terminal)	-28.0 ppm	0.8	$(10°, 90°)$
C_α (C-terminal)	-35.0 ppm	0.2	$(25°, 73°)$
CO (N-terminal)	78.0 ppm	0.9	$(90°, 10°)$

inequivalent sites could be resolved under regular MAS conditions, and (2) significant dipolar exchange ridges were visible in static powder experiments. Even though the latter were visible for all of the samples presented here no tests were made to ensure that the complete randomization limit $\tau \gg T_1^{14N}$ had been achieved, and in that sense these results can be considered as preliminary. Still, Fig. 13 analyzes the local field lineshapes for the nitrogen-bound carbon sites of L-alanyl-L-alanine. All these slices show evidently bigger dipolar patterns than those of other sites not bonded to ^{14}N, and if it is assumed that nitrogen spins in this compound are fast relaxing—a likely possibility in view of the distinct shapes of the resolved 2D DEAR patterns—it becomes possible to establish the orientation of the ^{13}C chemical shift tensors with respect to the CN bond vectors (Table 2).

Figure 14 shows additional 2D local field data, extracted this

FIG. 13. Comparison between the experimental 2D local field contour plots extracted from the 3D VACSY/DEAR ^{13}C spectrum of L-alanyl-L-alanine for various indicated sites, and their best-fit simulations. These fits were carried out by visual comparison and their NMR coupling is summarized in Table 2.
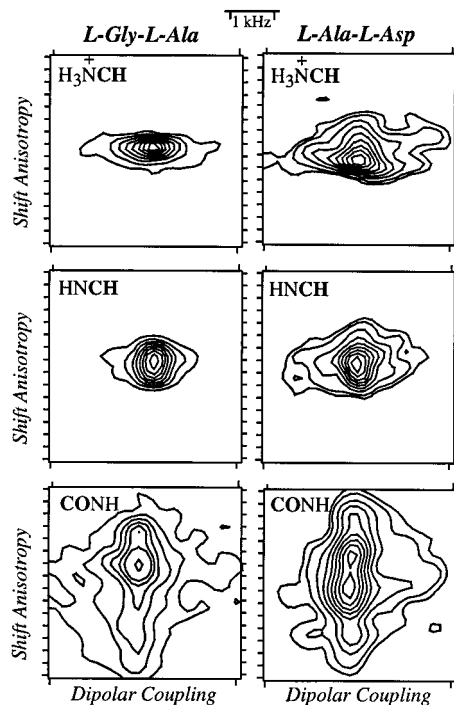

FIG. 14. 2D local field contour plots extracted for the indicated sites from the 3D spectra shown in Figs. 11 and 12.

time for various sites of L-glycyl-L-alanine and L-alanyl-L-aspartic acid. Again, the 2D exchange powder patterns are clearly broader along the dipolar dimensions among those carbons than are directly bonded to nitrogens; a complete characterization of these distinctive patterns is currently under way.

CONCLUSIONS

The main objective of this work was to describe some of the potential applications of relaxation-driven recoupling to the measurement of purely dipolar spectra. As a one-dimensional technique this approach allows one to measure a purely I–S dipolar spectrum; when extended to two dimensions it also enables one to orient this dipolar tensor within the principal axis framework of the S-spin local field; when incorporated into a variable-angle three-dimensional separation an experiment results which enables its application to complex molecular structures possessing several inequivalent chemical sites. These kinds of measurements have been available for some time for the case of spin-$\frac{1}{2}$ pairs based on the use of double-resonance irradiation techniques (7–9, 37, 38), but by relying on random rather than coherent fluctuations of the I-spin state the DEAR protocol opens up new possibilities regarding quadrupolar applications while avoiding the need for multiresonance spectrometers and probeheads. The technique is particularly applicable when the relaxation time of one of the spins is significantly shorter than that of the other, as the dipolar lineshapes become then independent of the I-spin relaxation or quadrupolar characteristics.

As examples of these concepts a series of applications was demonstrated on simple, nonlabeled powdered compounds containing ^{13}C–^{14}N spin pairs. Driving this choice of systems was their ubiquity, and the important role that according to recent theoretical investigations the relative sizes and orientations of C_α shielding tensors can play in determining the conformations of natural and synthetic polyamides (39, 40). Also in need of this type of information are certain recent solution-state NMR studies that extract macromolecular conformations based on the relative orientation of C_α's shielding and dipolar tensors in a molecular frame (41, 42). We trust that improvements on experiments like the ones here described plus their routine implementation might have a beneficial impact in these research areas as well.

APPENDIX

To properly simulate the 2D local field DEAR experiments described in this work the orientation dependence of the shielding and dipolar tensors need to be explicitly calculated. The chemical shift anisotropy is given by

$$\delta(\Omega) = \tfrac{1}{2}\Delta[(3\cos^2\theta_{CSA} - 1) + \eta\sin^2\theta_{CSA}\cos 2\varphi_{CSA}],$$
$$[A1]$$

where $\Omega = (\theta_{CSA}, \varphi_{CSA})$ describes the direction of the shielding tensor's principal axis system, and Δ, η are the coupling anisotropy parameters. The orientation dependence of the dipolar coupling is given by

$$\omega_D(\Omega') = d[3\cos^2\theta_{DD} - 1] = 2d\sqrt{\frac{4\pi}{5}}\, Y_{2,0}^{R\to D}(\theta_{DD}, 0),$$
$$[A2]$$

where d is the dipolar coupling constant given by $\gamma_I\gamma_S/4\pi r^3$ and θ_{DD} is the angle describing the orientation of the dipolar vector. Using Wigner rotation matrices we can relate this expression to the relative orientation of the shielding and dipolar tensors as

$$\omega_D = 2d\sqrt{\frac{4\pi}{5}}\sum_{m=-2}^{2} D_{m,0}^{(2)}(0, \theta_{CSA}, \varphi_{CSA})Y_{2,m}(\chi, \varphi), \quad [A3]$$

where χ and φ are the polar angles orienting the internuclear I–S vector within the shielding's principal axis system. This equation is explicitly given in terms of trigonometric functions by

$$\omega_D = \tfrac{1}{2}d\{3\sin^2\theta_{CSA}\sin^2\chi\cos[2(\varphi_{CSA} + \varphi)]$$
$$- 12\sin\theta_{CSA}\cos\theta_{CSA}\sin\chi\cos\chi\cos(\varphi_{CSA} + \varphi)$$
$$+ [3\cos^2\theta_{CSA} - 1][3\cos^2\chi - 1]\}. \quad [A4]$$

Equations [A1] and [A4] were used in the DEAR simulations shown in Figs. 7 and 13.

ACKNOWLEDGMENTS

REFERENCES

1. B. Blümich and R. Kosfeld (Eds.), "NMR: Basic Principles and Progress," Vols. 30–33, Springer-Verlag, New York (1994).

2. T. Guillon and J. Schaefer, *Adv. Magn. Reson.* **13,** 57 (1989).

3. A. E. Bennett, R. G. Griffin, and S. Vega, *in* "NMR: Basic Principles and Progress" (B. Blümich and R. Kosfeld, Eds.), Vol. 33, pp. 1–77, Springer-Verlag, New York (1994).

4. M. Baldus, D. G. Geuts, and B. H. Meier, *Solid State NMR* **11,** 157 (1998).

5. D. E. Kaplan and E. L. Hahn, *J. Phys. Radium* **19,** 821 (1958).

6. M. Emshwiller, E. L. Hahn, and D. E. Kaplan, *Phys. Rev.* **118,** 414 (1960).

7. R. K. Hester, J. L. Ackerman, B. L. Neff, and J. S. Waugh, *Phys. Rev. Lett.* **36,** 1081 (1976).

8. M. E. Stoll, A. J. Vega, and R. W. Vaughn, *J. Chem. Phys.* **65,** 4093 (1976).

9. M. Linder, A. Hohener, and R. R. Ernst, *J. Chem. Phys.* **73,** 4959 (1980).

10. D. P. Raleigh, M. H. Levitt, and R. G. Griffin, *Chem. Phys. Lett.* **146,** 71 (1988).

11. M. Engelsberg and C. S. Yannoni, *J. Magn. Reson.* **88,** 393 (1990).

12. R. Tycko and G. Dabbagh, *Chem. Phys. Lett.* **173,** 461 (1990).

13. C. P. Gray and W. S. Veeman, *Chem. Phys. Lett.* **192,** 379 (1992).

14. T. Guillon, *J. Magn. Reson. A* **117,** 326 (1995).

15. J. R. Sachleben, V. Frydman, and L. Frydman, *J. Am. Chem. Soc.* **118,** 9786 (1996).

16. L. Frydman, G. C. Chingas, Y. K. Lee, P. J. Grandinetti, M. A. Eastman, G. A. Barrall, and A. Pines, *J. Chem. Phys* **97,** 4800 (1992).

17. C. P. Slichter, "Principles of Nuclear Magnetic Resonance," Springer-Verlag, New York (1990).

18. J. Jeener, B. H. Meier, P. Bachmann, and R. R. Ernst, *J. Chem. Phys.* **71,** 4546 (1979).

19. N. M. Szeverenyi, M. J. Sullivan, and G. E. Maciel, *J. Magn. Reson.* **47,** 462 (1982).

20. A. Abragam, "The Principles of Nuclear Magnetism," Oxford Univ. Press, Oxford (1985).

21. C. A. Coulson, *Proc. R. Soc. (London) A* **164,** 383 (1938).

22. R. Tycko, G. Dabbagh, and P. A. Mirau, *J. Magn. Reson.* **85,** 265 (1989).

23. A. Bax, N. M. Szeverenyi, and G. E. Maciel, *J. Magn. Reson.* **52,** 147 (1983).

24. Z. H. Gan, *J. Am. Chem. Soc.* **114,** 8307 (1992).

25. J. Z. Hu, W. Wang, F. Liu, M. S. Solum, D. W. Alderman, R. J. Pugmire, and D. M. Grant, *J. Magn. Reson. A* **113,** 210 (1995).

26. L. Frydman, G. C. Chingas, Y. K. Lee, P. J. Grandinetti, M. A. Eastman, G. A. Barrall, and A. Pines, *Isr. J. Chem.* **32,** 161 (1992).

27. L. Frydman, Y. K. Lee, L. Emsley, G. C. Chingas, and A. Pines, *J. Am. Chem. Soc.* **115,** 4825 (1993).

28. L. Frydman, S. Vallabhaneni, Y. K. Lee, and L. Emsley, *J. Chem. Phys.* **101,** 111 (1994).

29. Y. K. Lee, L. Emsley, R. G. Larsen, K. Schmidt-Rohr, M. Hong, L. Frydman, G. C. Chingas, and A. Pines, *J. Chem. Phys.* **101,** 1852 (1994).

30. Y. K. Lee, R. L. Vold, G. L. Hoatson, and A. Pines, *J. Magn. Reson. A* **112,** 112 (1995).

31. Tecmag Inc., Houston, TX.

32. Courtesy of Professor P. Grandinetti, Ohio State University.

33. O. B. Peersen, X. L. Wu, I. Kustanovich, and S. O. Smith, *J. Magn. Reson. A* **104,** 334 (1993).

34. D. J. States, R. A. Haberkorn, and D. J. Ruben, *J. Magn. Reson.* **48,** 286 (1982).

35. M. S. Lehman, T. F. Koetzle, and W. C. Hamilton, *J. Am. Chem. Soc.* **94,** 2657 (1972).

36. A. Naito, S. Ganapathy, K. Akasake, and C. A. McDowell, *J. Chem. Phys.* **74,** 3190 (1981).

37. A. Ramamoorthy, L. M. Gierasch, and S. J. Opella, *J. Magn. Reson. B* **110,** 102 (1996).

38. J. Z. Hu, D. W. Alderman, R. J. Pugmire, and D. M. Grant, *J. Magn. Reson.* **126,** 120 (1997).

39. A. C. d. Dios, J. G. Pearson, and E. Oldfield, *Science* **260,** 1491 (1993).

40. A. C. d. Dios, and E. Oldfield, *Solid State NMR* **6,** 101 (1996).

41. N. Tjandra and A. Bax, *J. Am. Chem. Soc.* **119,** 9576 (1997).

42. M. Ottinger and A. Bax, *J. Am. Chem. Soc.* **120,** 12334 (1998).